LIGHT–MATTER INTERACTIONS ON THE FEMTOSECOND TIME SCALE

C. A. D. Roeser and E. Mazur
Department of Physics and Division of Engineering and Applied Sciences
Harvard University
9 Oxford St.
Cambridge, MA 02138 USA

Abstract The subject of electromagnetism in the presence of matter is both extensively studied and rich in diverse phenomena. It spans such topics as the quantization of the electromagnetic field to the semiclassical treatment of light–matter interactions to the derivation of the Fresnel reflectivity formulas. Interest in femtosecond optics is rooted in nonlinear optical phenomena and in the complex electron and lattice dynamics that occur in a material following intense ultrashort-pulse irradiation. The experiments we discuss are concerned mainly with the latter and lie at the crossroad of femtosecond optics and materials science, so-called ultrafast materials science.

1. Light–matter interactions

Fundamental to any description of light–matter interactions are Maxwell's equations [Haus, 1984],

$$\nabla \times \mathbf{E} = -\frac{\partial \mathbf{B}}{\partial t} \tag{1}$$

$$\nabla \times \mathbf{H} = -\frac{\partial \mathbf{D}}{\partial t} + \mathbf{J} \tag{2}$$

$$\nabla \cdot \mathbf{D} = \rho \tag{3}$$

$$\nabla \cdot \mathbf{B} = 0 \tag{4}$$

where, along with the usual field terms, $\mathbf{E}, \mathbf{D}, \mathbf{B}$, and $\mathbf{H}$, are the source terms of charge ρ and current $\mathbf{J}$. The influence of matter is cast in terms

of constitutive relations among the fields,

$$\mathbf{B} = \mu_0 \mu \mathbf{H} \tag{5}$$
$$\mathbf{D} = \epsilon_0 \epsilon \mathbf{E} \tag{6}$$
$$\mathbf{J} = \sigma \mathbf{E} \tag{7}$$

for which the vacuum (matter-less) conditions are $\mu \to 1$, $\epsilon \to 1$, and $\sigma \to 0$. As written, the equations are essentially linear, in that an applied $\mathbf{E}$ field of frequency ω generates a $\mathbf{D}$ field in the bulk of a material at ω and no other frequency. To isolate the response of the material, we introduce the polarization $\mathbf{P}$,

$$\mathbf{D} = \epsilon_0 \mathbf{E} + \mathbf{P} \tag{8}$$
$$\mathbf{P} = \epsilon_0 \chi^{(1)} \mathbf{E} \tag{9}$$

where the (linear) susceptibility $\chi^{(1)}$ is related to the dielectric constant by $\epsilon = \left(1 + \chi^{(1)}\right)$. Linear optical properties are fully described by either ϵ or $\chi^{(1)}$, which are complex, or by the complex index of refraction $\eta + i\kappa$.[1]

1.1 Relationship between linear optical properties and band structure

A detailed description of light-matter interactions, from a semiclassical or a quantum mechanical point of view, is quite satisfying when executed well and abysmal when not. Fortunately, we need not try to improve on success, and refer the reader to Refs. [Yu and Cardona, 1996] and [Cohen and Chelikowsky, 1989]. Our task, then, is to highlight the aspects of the semiclassical desciption of light-matter interactions that are of particular relevance for this article.

While the electromagnetic field is treated classically, the electrons are governed by the Hamiltonian [Yu and Cardona, 1996]

$$\mathcal{H} = \frac{\hat{\mathbf{p}}^2}{2m} + V(\hat{\mathbf{r}}) + \frac{e}{mc}\mathbf{A} \cdot \hat{\mathbf{p}} \tag{10}$$

where the first term is a kinetic energy term involving the momentum operator $\hat{\mathbf{p}}$, the second term is the electron–ion Coulomb interaction, and the third term encompasses the coupling between the applied field (represented by the vector potential $\mathbf{A}$) and the electrons.[2] The eigenstates of the above system in the absence of the perturbing field $\mathbf{A}$ are the well-known Bloch wavefunctions $|n, \mathbf{k}\rangle$, which in the position representation take the form

$$\langle \mathbf{r} | n, \mathbf{k} \rangle = u_{n,\mathbf{k}}(\mathbf{r}) e^{i(\mathbf{k}\cdot\mathbf{r})}. \tag{11}$$

Here, $u_{n,\mathbf{k}}(\mathbf{r})$ is a function with the periodicity of the lattice potential $V(\mathbf{r})$, and n and $\mathbf{k}$ corresponds to the band index and crystal momentum, respectively, in the reduced-zone scheme [Ashcroft and Mermin, 1976]. The energy eigenvalues $E_n(\mathbf{k})$ constitute the band structure of the crystal.[3] The difference between the band structures of different materials arises from differences in their lattice potentials, due to variations in composition, lattice configuration, or both. Of particular interest to the experiments described in Section 4 is the fact that a lattice potential that is changing in time gives rise to a time-varying band structure. Ultrashort laser pulses allow one to track the major features of the band structure via their manifestation in the linear optical properties of the material.

To investigate the interaction of light with the system described by Eq. (10), we consider the situation where the applied field excites electrons from an occupied (valence band) state to an unoccupied (conduction band) state. The number and energy distribution of such transitions give rise to the optical properties of a solid. Specifically, the imaginary part of the dielectric tensor can be written as [Yu and Cardona, 1996, Cohen and Chelikowsky, 1989]

$$\mathrm{Im}\left[\epsilon_i(\omega)\right] \sim \frac{1}{\omega^2} \sum_{n_\mathrm{c},n_\mathrm{v},\mathbf{k}} \delta\left(E_{n_\mathrm{c}}(\mathbf{k}) - E_{n_\mathrm{v}}(\mathbf{k}) - \hbar\omega\right) \left|\langle n_\mathrm{c},\mathbf{k}|\hat{\mathrm{p}}_i|n_\mathrm{v},\mathbf{k}\rangle\right|^2. \tag{12}$$

The momentum matrix element quantifies the strength of the coupling for vertical transitions between various conduction and valence band states.[4] The dependence of the momentum matrix element on the direction of the applied field, denoted by the subscript $i = x, y, z$, allows for an anisotropic optical response (*e.g.*, birefringence). The term common to all elements of the dielectic tensor is the joint density of states (JDOS)

$$\mathrm{JDOS} = \sum_{n_\mathrm{c},n_\mathrm{v},\mathbf{k}} \delta\left(E_{n_\mathrm{c}}(\mathbf{k}) - E_{n_\mathrm{v}}(\mathbf{k}) - \hbar\omega\right), \tag{13}$$

which depends solely on the shape of the band structure. The JDOS peaks at photon energies equal to the transition energy between many different states in $\mathbf{k}$ space. The fact that parallel conduction and valence bands produce a large peak in $\mathrm{Im}[\epsilon(\omega)]$ is a direct consequence of the form of the JDOS in Eq. (13). In fact, the linear optical response of many solids is dominated by only a few peaks in their JDOS — that is, by resonances at a small number of photon energies produced by only a few regions of parallel bands.

It is important to note that the correspondence between band structure and dielectric function is not one-to-one. Many band structures can

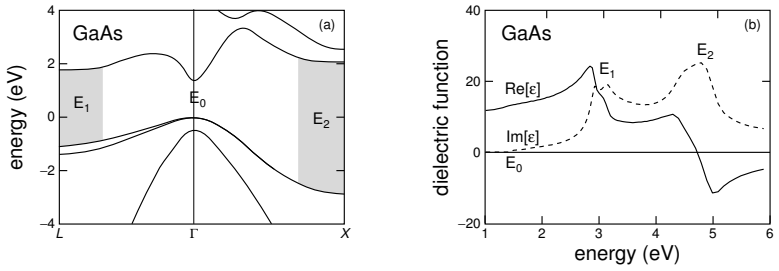

Figure 1. (a) Band structure [Cohen and Chelikowsky, 1989] and (b) dielectric function [Palik, 1985] of GaAs.

produce the same dielectric function,[5] which means that the interpretation of optical properties must be done cautiously. Changes in the linear optical properties can be used to make general statements about the changes in band structure, but additional information is often required to localize the dynamics in **k** space.

As an example of the direct relationship between band structure and dielectric function, Figure 1 shows the band structure and the dielectric function of GaAs. The characteristic absorption peaks in $\mathrm{Im}[\epsilon(\omega)]$ at 3.1 eV (E_1) and 4.7 eV (E_2) are due in part to a large joint densities of states around the L and X valleys, as indicated by the shaded regions in Figure 1(a). The real part shows the characteristic dispersive structure for each absorption peak, in agreement with the Kramers–Kronig relations.

1.2 The Drude–Lorentz model

The Drude–Lorentz model, also known as the Lorentz oscillator model when applied to semiconductors and as the Drude model when applied to metals, attempts to describe the optical response of a material as that of a classical harmonic oscillator. While simple, involving only a few free parameters, the Drude–Lorentz model is surprisingly good at describing the optical properties of many semiconductors and metals.

The Lorentz model describes, in a phenomenological way, the polarization induced in a material by the applied **E** field. The situation we consider is that of an electron in a solid that is described by its displacement x from its equilibrium position.[6] The equation of motion for the displacement x is taken to be that of a harmonic oscillator,

$$\frac{d^2}{dt^2}x + \Gamma\frac{d}{dt}x + \omega_0^2 x = F(t) \tag{14}$$

where Γ is a phenomenological damping coefficient, ω_0 is the resonance frequency of the oscillator (a real resonance in the material), and the driving force is due to the applied field,

$$F(t) = \frac{e}{m}\left[Ee^{-i\omega t} + E^* e^{i\omega t}\right]. \tag{15}$$

Without loss of generality, the equation of motion for $x(t)$ can be solved by neglecting the second driving term above and considering a trial solution of the form $x(t) = Ce^{-i\omega t}\ldots$

$$C[-\omega^2 - i\Gamma\omega + \omega_0^2]e^{-i\omega t} = \frac{e}{m}Ee^{-i\omega t} \tag{16}$$

$$\Rightarrow C = \frac{e}{m}E\frac{1}{\omega_0^2 - \omega^2 - i\Gamma\omega} \tag{17}$$

$$\Rightarrow x(t) = \frac{e}{m}E\frac{e^{-i\omega t}}{\omega_0^2 - \omega^2 - i\Gamma\omega}. \tag{18}$$

While $x(t)$ describes the motion of a single electron, it is often the case that many electrons in a solid respond in the same fashion. Thus, if N electrons respond as $x(t)$, then the total polarization is given by

$$P(t) = Nex(t) = \epsilon_0\chi^{(1)}E(t), \tag{19}$$

where Eq. (9) is used to relate the applied field $E(t)$ to the polarization $P(t)$ and to introduce the linear susceptibility. Hence,

$$\chi^{(1)} = \frac{Ne}{\epsilon_0}\frac{x(t)}{E(t)} = \frac{Ne^2}{\epsilon_0 m}\frac{1}{\omega_0^2 - \omega^2 - i\Gamma\omega}. \tag{20}$$

For our purposes, the dielectric function is more useful than the susceptibility, and takes the form,

$$\mathrm{Re}[\epsilon(\omega)] = 1 + f\frac{E_{\mathrm{res}}^2 - (\hbar\omega)^2}{(E_{\mathrm{res}}^2 - (\hbar\omega)^2)^2 + (\Gamma\cdot\hbar\omega)^2} \tag{21}$$

$$\mathrm{Im}[\epsilon(\omega)] = f\frac{\Gamma\cdot h\omega}{(E_{\mathrm{res}}^2 - (\hbar\omega)^2)^2 + (\Gamma\cdot\hbar\omega)^2}. \tag{22}$$

There are two methods by which the Lorentz model is applied to real absorbing materials. First, because the Lorentzian shape of $\mathrm{Im}[\epsilon_{\mathrm{Lorentz}}(\omega)]$ is similar to a δ-function, materials can be modeled by a distribution of Lorentz oscillators, analogous to the distribution of δ-function contributions to the JDOS in Eq. (13). The sum of many oscillators would produce a "single resonance" in the material (*e.g.*, the E_2 peak in GaAs).

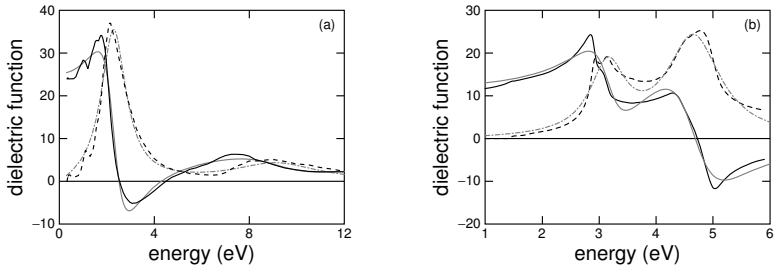

Figure 2. Lorentz oscillator model fits to (a) Te and (b) GaAs. Black lines represent literature values of Re[ϵ] (solid) and Im[ϵ] (dashed) [Palik, 1985], while gray lines represent the best-fit values of Re[$\epsilon_{\mathrm{Lorentz}}$] (solid) and Im[$\epsilon_{\mathrm{Lorentz}}$] (dash-dotted).

However, for modeling changes in the dielectric function on a femtosecond time scale, this technique is numerically challenging to implement (due to noise in the data) as well as physically unsatisfying in the interpretation of its results.

A second method of applying the Lorentz model to real materials is to describe an entire resonance by the three free parameters of a single oscillator; the resonant frequency ω_0, the linewidth Γ, and the oscillator strength $f = Ne^2/\epsilon_0 m$. Each parameter is connected to features of the band structure. The resonant frequency ω_0 corresponds to the position of the peak in the JDOS. The linewidth Γ is related to the distribution of energy levels around the resonant frequency — sharper absorption lines correspond to smaller values of Γ, arising from regions of parallel bands. Lastly, the oscillator strength f carries information about the number of states contributing to the resonance at ω_0.

As an example of the success of the Lorentz model in describing real materials, Figure 2 shows fits to Te and to GaAs. In each case, the fit is the sum of two Lorentz oscillators with different values of ω_0, Γ, and f for each term. This two-oscillator model follows the major features of the literature optical properties in each case, but fails to capture smaller features. For example, Im[$\epsilon_{\mathrm{Lorentz}}(\omega)$] does not vanish for photon energies below the band gap, nor is it sensitive to sharp features near other critical points. Nevertheless, the Lorentz model is sensitive to large resonances in a material — the parameters of the fit to GaAs in Figure 2(b) indicate resonances at 3.18 eV (E_1 peak) and 4.67 eV (E_2 peak).[7]

The form of the Drude model for metals is

$$\epsilon_{\mathrm{Drude}}(\omega) = 1 + \frac{Ne^2}{\epsilon_0 m}\left(\frac{i\tau}{\omega(1-i\omega\tau)}\right), \tag{23}$$

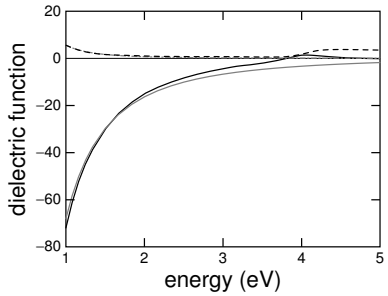

Figure 3. Drude model fit to Ag. Black lines represent literature values of Re[ϵ] (solid) and Im[ϵ] (dashed) [Palik, 1985], while gray lines represent the best-fit values of Re[$\epsilon_{\mathrm{Drude}}$] (solid) and Im[$\epsilon_{\mathrm{Drude}}$] (dash-dotted).

which is equivalent to Eqs. (21) and (22) with $\Gamma \to 1/\tau$ and $\omega_0 \to 0$. By convention, a plasma frequency is defined $\omega_{\mathrm{p}}^2 = Ne^2/\epsilon_0 m$ to play the role of the oscillator strength above. The classical derivation of $\epsilon_{\mathrm{Drude}}(\omega)$ is analogous to the above derivation for $\epsilon_{\mathrm{Lorentz}}(\omega)$, except that an induced current $\mathbf{J}$ rather than an induced polarization $\mathbf{P}$ results in a differential equation that lacks a harmonic potential term [Ashcroft and Mermin, 1976]. The optical properties of many metals consist of a Drude (intraband) contribution from "free" electrons in half-filled bands in addition to Lorentz oscillator (interband) contributions from available vertical transitions. That is, even good metals are rarely described by the Drude model alone. To illustrate this fact, Figure 3 shows a Drude model fit to Ag, with $\omega_{\mathrm{p}} = 8.3$ eV and $\tau = 50$ fs. While the fit describes low-photon-energy behavior well, it is not accurate near 4 eV due to resonance contributions to $\epsilon(\omega)$.

1.3 The Kramers–Kronig relations

Thus far we have discussed both the real and the imaginary part of the dielectric function as if the two quantities were independent. In reality, Re[$\epsilon(\omega)$] and Im[$\epsilon(\omega)$] are linked through the Kramers–Kronig relations [Jackson, 1975]

$$\mathrm{Re}[\epsilon(\omega)] = 1 + \frac{2}{\pi}\mathcal{P}\int_0^\infty \mathrm{d}\nu\, \frac{\nu\,\mathrm{Im}[\epsilon(\nu)]}{\nu^2 - \omega^2} \tag{24}$$

$$\mathrm{Im}[\epsilon(\omega)] = \frac{2\omega}{\pi}\mathcal{P}\int_0^\infty \mathrm{d}\nu\, \frac{1 - \mathrm{Re}[\epsilon(\nu)]}{\nu^2 - \omega^2} \tag{25}$$

where $\mathcal{P}$ represents the principal value of the integral. It is worth noting that the Kramers–Kronig relations follow from the fact that the electric

field **E** drives the material polarization **P**, as in Eq. (9) [Jackson, 1975]. Interestingly, the availability of transitions at a single photon energy contributes locally to $\mathrm{Im}[\epsilon(\omega)]$ (see Eq. (12)) but affects $\mathrm{Re}[\epsilon(\omega)]$ globally according to the Kramers–Kronig relations. For fitting dielectric function data to the Lorentz model when some of the material resonances lie outside the measured spectal range, the expression for the imaginary part will fit the data correctly due to the local contribution of transitions, but the real part will have unaccounted-for global contributions. It is often the case that an additive constant to the real part can dramatically improve the fit by playing the role of these Kramers–Kronig-type contributions from resonances outside the detected spectral range. Since the real part of the Lorentz model is mostly constant far from a resonance,[8] a single additive-constant free parameter is often sufficient to capture all the resonance contributions to $\mathrm{Re}[\epsilon(\omega)]$ from outside the spectral range of the data.

2. Ultrafast dynamics of solids under intense photoexcitation

Despite the broad array of topics that fall under the title "ultrafast dynamics of solids," the discussion below is of limited range. For instance, we do not discuss the myriad of electronic phenomena that have been observed at low excitation densities of 10^{14} to 10^{18} cm^{-3}, a review of which can be found in Ref. [Shah, 1996]. The reason for this omission is that such phenomena are rarely observed in experiments where the excited carrier density is on the order of 10^{22} cm^{-3}. Although excited carrier effects are present and are more pronounced than at lower densities, the material dynamics are often dominated by the ionic motion that results from excitation of a significant fraction of the valence electrons. The text that follows is an attempt to present the framework in which these dynamics are understood.

2.1 Molecular dynamics and coherent control

The idea that solid dynamics are determined by ionic motion is rooted in the microscopic picture of molecular electronic transitions and molecular dynamics. In fact, the molecular case is even more extreme than the solid one — photoexcitation in molecules often results in dissociation, whereas the sharing of electrons in a solid leads to only a partial weakening of bonds under photoexcitation.[9] Consider a diatomic sodium molecule, where the energy of the system as a function of nuclear displacement is as shown in Figure 4. The curves in this figure show the energy of the system in different electronic configurations as a function

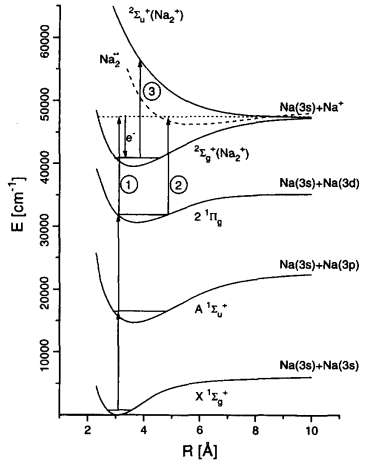

Figure 4. Potential energy curves for a diatomic sodium molecule, showing bond stretching or dissociation for different excited state potentials. Numbers 1, 2 and 3, indicate the possible transitions to products in a two-pulse excitation scheme after the first pulse excites the electronic system to $2\,^1\Pi_g$. After Ref. [Assion et al., 1996].

of ionic separation. Often, the excited state potentials have a shape that results in dissociation (no minimum at finite separations) or bond stretching (a minimum at a different separation than the ground state). When this is the case, electronic transitions are coupled to molecular vibrational transitions [Atkins, 1983], where our intuition predicts that the ensuing nuclear motion is determined by the new potential in a classical way — an excitation from the ground $X\,^1\Sigma_g^+$ state to the $2\,^1\Pi_g$ state of Figure 4 would leave the nuclei displaced from equilibrium and they will thus begin to oscillate. The idea that the nuclei remain fixed during the electronic transition[10] is equivalent to the approximation of vertical transitions in crystals and is known as the Franck-Condon principle [Atkins, 1983].

The quantum mechanical derivation of molecular excited state dynamics was first provided by Heller [Heller, 1978, Heller, 1981]. To summarize, immediately after photoexcitation, the ground nuclear eigenstate evolves on the excited state potential surface following the classical trajectory. The anharmonicity of the excited state potential determines the rate at which the nuclear wavepacket spreads and leads to deviations from the classical trajectory. Of primary interest in our case is understanding the way in which the resulting nuclear dynamics can af-

fect properties such as the dielectric function. Heller points out the lack of such a description at the time, stating

> After the electrons have made a transition, the nuclei experience new forces; they find themselves displaced relative to the equilibrium geometry of the new potential surface, and interesting dynamics should ensue. Unfortunately, most discussions of electronic transitions cut short any allusions to dynamics and explain the absorption spectrum in terms of Franck-Condon overlaps of the initial nuclear wavefunction with a time-independent vibrational *eigenfunction* of the upper electronic potential surface. We (and the nuclear wave function) are left hanging; we are given no explanation of the time evolution of the hapless nuclei which, once the photon is absorbed, are ready to move in ways that *determine* the spectra [Heller, 1981].

Before making the connection between molecular and crystal dynamics, we discuss an important application of Heller's work — the coherent control of molecular dissociation. Tannor, Kosloff, and Rice devised a scheme under which the dissociation dynamics of a hypothetical molecule can be controlled simply by varying the time delay between two femtosecond pulses [Tannor et al., 2086, Rice and Zhao, 2000]. They considered a ground state potential energy surface with one bound state (ABC) and two dissociated states (AB + C, A + BC), along with different excited state potential surfaces. They demonstrated that by allowing the nuclear wave function to propagate on the excited state potential for specific (different) lengths of time before the second pulse arrives, the "final product" of the two-pulse excitation can be controlled.[11] Experimental realizations of end-product control in molecular dissociation (in systems such as that of Figure 4) have been achieved with multiple-pulse and shaped-pulse excitations [Assion et al., 1996, Brixner et al., 2001].

2.2 The molecular picture of crystal dynamics

Many of the features of the dynamics of solids can be understood within the framework described above, albeit with some extensions. Photoexcitation of a large density of electrons establishes a new potential energy surface on which the ions move. The new potential may have no minimum near the initial lattice configuration, resulting in large nuclear displacements, disordering, and often "damage." If a new potential minimum is established, then the ions can respond to the new potential in a more controlled fashion. Nuclear motion on the new potential energy surface leads to commensurate changes in the band structure, and, in turn, in the optical properties of the solid. That is, the available transitions for the electrons are determined by the lattice configuration, the dynamics of which are determined by the excited electrons.

Additional considerations when discussing solids concern the treatment of the "excited electronic state." First, the manifold of excited energy states is virtually a continuous function of the excited electron density. In general, the excited electron density cannot specify an unique potential because of the possible permutations of transitions among the 10^{23} cm^{-3} valence electrons. The idea that material dynamics depend on the excited electron density alone is an approximation that holds when the carriers can thermalize before any significant nuclear motion occurs. Excited electrons (holes) thermalize within 10 fs at densities of 10^{21} cm^{-3} or more,[12] leading to a Fermi-Dirac distribution within the conduction (valence) band and a loss of memory of the initial excited carrier configuration. Because the ions spend most of their time (all but 10 fs) evolving on a potential determined by a Fermi-Dirac distribution of carriers, the excited electron density is often sufficient to specify the "excited electronic state." A second concern is that the electronic state and the nuclear state do not evolve independently. A particular excited electron distribution establishes a potential surface to which the lattice responds by deformation. This deformation results in a new band structure, resulting in a redistribution of electrons and, in general, a modified potential. In essence, the excited electron potential becomes a dynamic quantity which depends on the nuclear coordinates. These many-body interactions are more pronounced in solids than in molecules and can dynamically modify the potential energy surface and further perturb the semiclassical trajectories of the ions. Electron-electron interactions of exchange and correlation, electron-phonon interactions, and other many-body interactions offer avenues by which the electron distribution within a band can exert a force on the ions.

Even with the further complications of dealing with solids, nuclear dynamics can still be treated with excited state potential surfaces. The accuracy of "exact" calculated results for solids will be less than for molecules, simply due to the increased complexity of a condensed system. Usually, approximations to reduce the complexity of the system make the problem tractable and model a specific experimental situation. We present an example of such a treatment in the following section.

2.3 Ultrafast disordering of zincblende semiconductors

The observation of laser-induced disordering on a time scale shorter than the thermalization time between excited carriers and the lattice was observed by a number of groups working with semiconductors [Shank et al., 1983b, Tom et al., 1988, Govorkov et al., 1991, Saeta et al.,

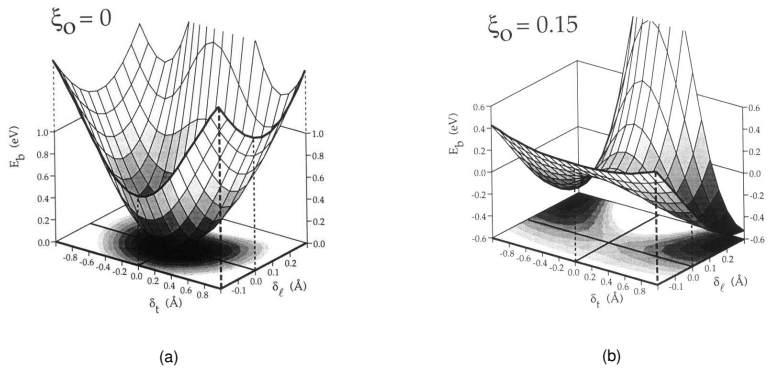

Figure 5. Potential energy surface as a function of transverse acoustic (δ_t) and longitudinal optical (δ_l) lattice displacements for silicon (a) in the ground state electronic configuration and (b) when 15% of valence electrons are excited to the conduction band. The stable minimum at $\delta_t = \delta_l = 0$ becomes unstable for sufficient excitation densities, as shown here. After Ref. [Stampfli and Bennemann, 1994].

1991, Sokolowski-Tinten et al., 1991]. Although the disordering of solids via thermal processes (*i.e.*, melting) has been known for a long time, a theoretical description of lattice instability as a result of photoexcitation was first provided by Stampfli and Bennemann [Stampfli and Bennemann, 1990, Stampfli and Bennemann, 1994]. Apparently derived independently from the work described above, their treatment of zincblende semiconductors shares many features with the molecular description of nuclear motion on an excited state potential.

Stampfli and Bennemann consider a tight-binding Hamiltonian that includes nearest-neighbor interactions only. A calculation of the potential surface for the lattice in the ground electronic state configuration is shown for silicon in Figure 5(a). A clear minimum exists as a function of transverse acoustic (δ_t) and longitudinal optical (δ_l) lattice distortions, indicating a stable lattice. The band structure and optical properties of the calculated ground state configuration agree well with the known properties of Si. After photoexcitation, the excited electrons rapidly take on a Fermi-Dirac distribution[13] and the lattice potential is recalculated with the different band-filling. As shown in Figure 5(b), when 15% of valence electrons are excited to the conduction band,[14] the lattice potential no longer displays a stable minimum at the ground state lattice configuration. The calculated trajectory of the ions is shown in Figure 6, displaying oscillations and translation in one direction and pure translation in another, following the shape of the potential in Figure 5(b). The significant motion of ions on a time scale of 100 fs agrees with the

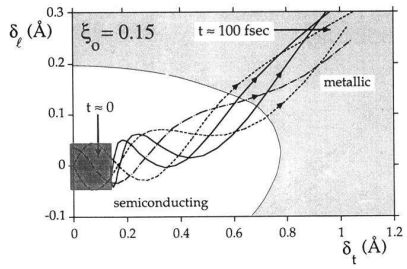

Figure 6. Trajectory of ionic motion on the potential shown in Figure 5(b). Significant nuclear displacements are predicted to occur within 100 fs. After Ref. [Stampfli and Bennemann, 1994].

experimental results of many groups [Shank et al., 1983b, Tom et al., 1988, Govorkov et al., 1991, Saeta et al., 1991, Sokolowski-Tinten et al., 1991], and the onset of metallic behavior on this time scale has also been observed [Callan et al., 1998, Callan et al., 2001a].

The main difference between the response of silicon and that of Na_2 molecules to photoexcitation is that an ensemble of ions, rather than two, are set in motion on a new potential surface. As shown in Figure 6, the ionic motion is confined to a certain path for all initial conditions (within a certain range). As discussed in Section 4, the physical mechanisms underlying the response of tellurium to intense photoexcitation are similar to those that govern the response of silicon. Whereas nuclear motion in silicon develops along two directions, the photoinitiated nuclear motion in tellurium affects only a single lattice parameter. Moreover, the excited state potential in tellurium has a minimum near the initial lattice configuration, which leads to lattice vibrations that are analogous to the vibrations observed in Na_2.

3. Nonlinear optical properties

Although the majority of this article concerns linear optics in solids, nonlinear optical processes are encountered as well. A nonlinear optical response occurs when fields of frequency different than that of the applied field are generated. The nonlinear response is usually isolated from the linear one, and Eq. (9) becomes

$$\mathbf{P} = \epsilon_0 \chi^{(1)} \mathbf{E} + \mathbf{P}^{NL} \tag{26}$$

$$\mathbf{P}^{NL} = \epsilon_0 \chi^{(2)} : \mathbf{E} \cdot \mathbf{E} + \epsilon_0 \chi^{(3)} :: \mathbf{E} \cdot \mathbf{E} \cdot \mathbf{E} + \cdots . \tag{27}$$

Essentially, the material response is expanded in powers of the applied $\mathbf{E}$ field. Note that the total field is involved in driving the polariza-

tion and this total field may involve contributions from laser pulses of different frequency travelling in different directions with different field polarizations. The total polarization then acts as a driving term, as in Eq. (8), to radiate fields at the fundamental frequency[15] as well as at the frequency of the nonlinear polarization.

Broadly speaking, there are two criteria which must be satisfied in order to generate nonlinear radiation. For a nonlinear process involving n fields of the form[16]

$$E_j(t) = \frac{1}{2}\left(E_j e^{i(\vec{k}_j\cdot\mathbf{r}-\omega_j t)} + E_j^* e^{-i(\vec{k}_j\cdot\mathbf{r}-\omega_j t)}\right), \tag{28}$$

for $j = 1 \ldots n$, these criteria are

$$\omega_{NL} = \sum_{i=1}^{n} \pm\omega_i \tag{29}$$

$$\vec{k}_{NL} = \sum_{i=1}^{n} \pm\vec{k}_i \tag{30}$$

where the choice of sign indicates whether the "ω" or the "$-\omega$" term of a particular field contributes, as determined by the particular nonlinear process considered and the experimental arrangement. Equation (29) is always satisfied in a nonlinear process and specifies the nonlinear frequency generated. Equation (30) is the "phase-matching" condition and determines the direction of the radiated nonlinear field.[17] In the remainder of this Section, we present an overview of second- and third-order nonlinearities and refer the interested reader to Ref. [Boyd, 2003] for further details.

3.1 Second-order nonlinearities

The type of second-order nonlinear process most often encountered in the lab is second harmonic generation (SHG), which involves two degenerate driving fields ($\omega_1 = \omega_2$) of the form in Eq. (28). The nonlinear polarization generated by SHG is

$$P^{(2)}(2\omega_1) = \epsilon_0\chi^{(2)}(2\omega_1 : \omega_1, \omega_1)E_1E_1e^{i\left(\vec{k}(2\omega_1)\cdot\mathbf{r}-2\omega_1 t\right)} \tag{31}$$

where the criteria of Eqs. (29) and (30) involve only positive terms (*e.g.*, $\omega_{NL} = \omega_1 + \omega_1$). We have allowed for less-than-perfect phase matching because the dispersion of the material determines whether $\vec{k}(2\omega_1) = 2\vec{k}(\omega_1)$. When the phase matching is not perfect, the nonlinear field generated at different positions in the crystal intefere somewhat destructively, reducing the total radiated nonlinear field.

The most common application of SHG is in measuring the duration of a femtosecond pulse via autocorrelation. In practice, two copies of the same pulse are overlapped in a nonlinear crystal with a controllable delay τ between the two pulses. Because the nonlinear field depends on the total intensity, the SHG signal S varies with the temporal overlap of the pulses. One can extract the pulse duration from the shape of $S(\tau)$.[18]

3.2 Third-order nonlinearities

In general, third-order nonlinearities require three driving fields. In practice, two or even all three fields are degenerate. One situation of particular interest is the following interaction between two fields of frequency ω_1 and ω_2

$$P^{(3)}(\omega_{NL}) = \frac{1}{2}\epsilon_0\chi^{(3)}(\omega_{NL}:\omega_1,-\omega_1,\omega_2)E_1E_1^*E_2e^{i\left(\vec{k}_2\cdot\mathbf{r}-\omega_2 t\right)} \quad (32)$$

$$\omega_{NL} = \omega_1-\omega_1+\omega_2 \quad (33)$$

$$\vec{k}_{NL} = \vec{k}_1-\vec{k}_1+\vec{k}_2 \quad (34)$$

This particular nonlinear mixing can result in intensity-dependent effects. For $\chi^{(3)}$ real, an intensity-dependent index of refraction leads to self-focussing of a gaussian beam.[19] An imaginary $\chi^{(3)}$ produces intensity-dependent absorption (*i.e.* two-photon absorption). Both phenomena are widely applied in the field of optics. Self-focussing, or Kerr lensing, is used to mode-lock oscillators and contributes to the generation of white-light femtosecond pulses. Two-photon absorption (TPA) is commonly used for cross-correlation of ultrashort pulses because it is automatically phase-matched and produces a field at the fundamental.

Of particular interest to researchers is how nonlinear susceptibilities are related to (and can reveal) material properties. For instance, the process of two-photon absorption described in Eq. (32) does not occur unless a photon of energy $\hbar(\omega_1+\omega_2)$ would be absorbed linearly. This is not to say that $\mathrm{Im}[\chi^{(3)}]$ depends on $\mathrm{Im}[\chi^{(1)}]$. Rather, both depend on the availability and distribution of, in this case, vertical electronic transitions.

In addition to electronic transitions, the existence of lattice vibrations (phonons) serves to enhance nonlinear susceptibilities, in particular $\chi^{(3)}$, via the change in linear optical properties with lattice distortion. When the interaction in Eq. (32) is used to probe (or excite) a phonon ω_v of a solid where $\omega_1-\omega_2=\omega_\mathrm{v}$, it is called a Raman interaction. The form of the phonon contribution to the nonlinear susceptibility is given by

[Boyd, 2003]

$$\chi^{(3)}_{\text{Raman}}(\omega_2 : \omega_1, -\omega_1, \omega_2) \sim \left(\frac{\partial \alpha}{\partial q}\right)^2 \frac{1}{\omega_{\text{v}}^2 - (\omega_1 - \omega_2)^2 + 2i\,(\omega_1 - \omega_2)\,\gamma}\,, \tag{35}$$

where q is a displacement of the lattice associated with the phonon and γ is the associated damping constant. By convention, ω_2 is referred to as the Stokes frequency when $\omega_2 < \omega_1$ and as the anti-Stokes frequency otherwise. The quantity α is the polarizability of the material, which changes as the lattice is distorted. Note that $\chi^{(3)}_{\text{Raman}}$ contains a resonance denominator of similar form to the linear susceptibility in Eq. (20), however the "strength" of the Raman process depends on the sensitivity of the polarizability to lattice displacement. Analogous to the electronic case, where an applied field induces an oscillating electronic polarization that leads to excitation of an electron, Raman interactions lead to the excitation of phonons.

4. Ultrafast Materials Science

Early investigations into ultrafast materials science relied on intense femtosecond laser pulses to initiate and probe dynamics that follow from photoinduced lattice instabilities [Shank et al., 1983b, Shank et al., 1983a]. Recently, the focus has shifted from photoinduced instabilities that lead to a disordered state [Saeta et al., 1991, Govorkov et al., 1991, Sokolowski-Tinten et al., 1991] to those that result in an altered lattice configuration [Misochko et al., 1999, Cavalleri et al., 2001, Sokolowski-Tinten et al., 1998] and to the methods by which lattice dynamics can be controlled [Wefers et al., 1995, Hase et al., 1996, Bartels et al., 1998, DeCamp et al., 2001]. As discussed in Section 2, the nuclear motion is believed to follow a trajectory dictated by the potential surface of the electronic excited state [Stampfli and Bennemann, 1994], much like the semiclassical picture of nuclear dynamics in molecules [Heller, 1978, Tannor et al., 2086, Assion et al., 1996, Brixner et al., 2001].

In this Section, we discuss the electron and lattice dynamics of a variety of semiconductors following excitation by an intense femtosecond laser pulse. We observe these dynamics by measuring the dielectric tensor of the material with femtosecond time resolution. The linear optical properties of a material provides a view of the underlying band structure and lattice configuration that the reflectivity of a sample alone cannot. Consequently, measurements of the femtosecond time-resolved dielectric tensor provide a greater amount of information about electron and lattice dynamics and about the nature of ultrafast phase transitions than other optical probes.

We performed pump–probe experiments on commercially available GaAs, on *a*-GeSb thin films, and on single-crystal tellurium using 800-nm pulses from a multipass amplified Ti:sapphire laser, producing 0.5-mJ, 35-fs pulses at a repetition rate of 1 kHz [Backus et al., 1995]. In each case, s polarized pump pulses excite the sample while the p polarized transient reflectivity is measured using a white-light pulse (1.65 – 3.2 eV). Two-photon absorption measurements [Albrecht et al., 1991] indicate that the time-resolution of the pump–probe setup is better than 50 fs, while calculations based on measurements of the spectrum and chirp of the white-light probe indicate that the time resolution of the probe varies from 20 fs near 1.7 eV to 60 fs near 3.2 eV [Kovalenko et al., 1999]. The entire system is calibrated to obtain absolute reflectivity. Measurements of the absolute reflectivity at two angles of incidence allow for determination of the linear optical properties by numerical inversion of the Fresnel formulas. Further details of this experimental technique can be found in Ref. [Roeser et al., 2003].

4.1 Ultrafast carrier and lattice dynamics in GaAs

Shortly after the introduction of femtosecond laser sources, numerous experiments were conducted on semiconductors where a transition to a metallic state was observed upon laser irradiation. Experimental techniques included pump–probe reflectivity measurements [Shank et al., 1983b], both reflectivity and second harmonic measurements [Shank et al., 1983a, Saeta et al., 1991, Tom et al., 1988, Govorkov et al., 1991], and pump–probe microscopy [Downer et al., 1985, Sokolowski-Tinten et al., 1998]. While a laser-induced phase transition was observed in each experiment with high precision, the nature of the resulting phase and the changes in the band structure were difficult to determine. This difficulty is due to the fact that many different values of $\epsilon(\omega)$, and hence many different band structures and material phases, can yield the same reflectivity at a particular angle of incidence.

We performed single-shot femtosecond time-resolved dielectric function measurements of GaAs to investigate carrier and lattice dynamics associated with its ultrafast semiconductor-to-metal transition under intense photoexcitation [Callan et al., 1998, Huang et al., 1998]. Figure 7 shows dielectric function measurements of GaAs. Without excitation of the sample, $\epsilon(\omega)$ matches literature values of the dielectric function [Palik, 1985], confirming that our technique measures the dielectric function correctly. Figure 7(b) shows $\epsilon(\omega)$ 500 fs after excitation below the threshold for permanent damage ($F_{\mathrm{th}} = 1.0$ kJ/m^2). Shortly after exci-

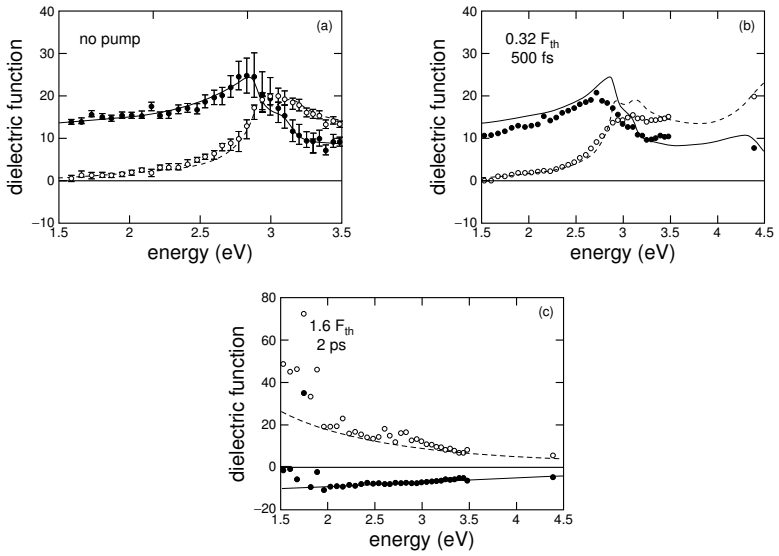

Figure 7. Dielectric function data for GaAs — • = Re[ϵ], ∘ = Im[ϵ]. (a) Under no excitation, $\epsilon(\omega)$ matches literature values of the dielectric function, represented by the solid and dashed curves [Palik, 1985]. An example of changes in $\epsilon(\omega)$ due to the presence of excited carriers is shown in (b). (c) At sufficiently high pump fluences, a semiconductor-to-metal transition is observed, as evidenced by the fit to the Drude model ($\omega_{\rm p} = 13.0$ eV and $\tau = 0.18$ fs).

tation, before the ions of the lattice can move, changes in $\epsilon(\omega)$ are due to the presence of excited carriers in the conduction band. The decrease of Im[$\epsilon(\omega)$] around the E_1 critical point (near 3 eV) is likely due to Pauli blocking of the transition by electrons in the conduction band. At higher excitation fluences, a transition to a metallic state is observed, an example of which is shown in Figure 7(c). This data is well fit by the Drude model, which describes free-electron (metallic) behavior. The parameters of the fit (a plasma frequency of 13 eV and a relaxation time of 0.18 fs) reveal that virtually all of the valence electrons are free and that the band gap has completely collapsed. Theoretical calculations of the evolution of the dielectric function of GaAs after femtosecond-pulse excitation agree with our experimental results [Graves and Allen, 1998, Allen et al., 2000, Benedict, 2001].

4.2 Ultrafast phase changes in *a*-GeSb

The speed of ultrafast phase transitions and the large reflectivity variations associated with them make materials that display such transitions

good candidates for optical switches and high speed optical data storage. Thin films of *a*-GeSb allow optically induced, optically reversible amorphous-to-crystalline transitions. In 1998, Sokolowski-Tinten and co-workers presented normal-incidence reflectivity measurements which suggested that femtosecond pulses above the threshold for permanent crystallization can induce an ultrafast *disorder-to-order* transition in amorphous $Ge_{0.06}Sb_{0.94}$ films within 200 fs [Sokolowski-Tinten et al., 1998]. The suggestion of a subpicosecond amorphous-to-crystalline phase transition raises an important question: how can lattice ordering occur in less time than it takes to establish thermal equilibrium between the laser-excited electrons and the lattice?

We performed single-shot dielectric function measurements of a 50-nm thin film of *a*-$Ge_{0.06}Sb_{0.94}$ to determine the nature of the phase during its ultrafast phase transition [Callan et al., 2001b]. Figure 8(a) shows the agreement between $\epsilon(\omega)$ obtained at a time delay of -1 ps and literature values of the dielectric function [Palik, 1985]. As a reference, the dielectric function of the crystalline phase is also shown.[20] Because the film was optically thin and covered by a 1.25-nm SbO_2 oxide layer [de Sande et al., 1994], this sample is considered a four-medium system: air, oxide, *a*-GeSb thin film, and fused silica substrate.

Figure 8(b) shows the response of the dielectric function 200 fs after arrival of a pump pulse of fluence $F = 320$ J/m^2, which is 60% above the threshold for permanent crystallization ($F_{\rm cr}$). At this excitation fluence, the dielectric function remains unchanged from 200 fs to 475 ps. The same dielectric function is observed on subpicosecond time scales for all fluences above F_{cr}, indicating the existence of a nonthermal phase after femtosecond-pulse excitation. The existence of a new phase at ultrashort time delays for all fluences above $F_{\rm cr}$ was correctly identified by the authors of Ref. [Sokolowski-Tinten et al., 1998], however, the material is not crystalline, as evidenced by the discrepancy between the measured dielectric function and that of the crystalline phase (see Figure 8(b)). This discrepancy is brought out by Figure 8(c), which shows the normal-incidence reflectivity as calculated from our time-resolved dielectric function measurements. Only at the 2.01-eV photon energy of the experiments in Ref. [Sokolowski-Tinten et al., 1998] does the reflectivity at 200 fs after excitation above $F_{\rm cr}$ match that of the crystalline phase. Furthermore, even at 2.01 eV, we find that for angles of incidence near or above the pseudo-Brewster, the reflectivity does not go to the crystalline level for pump fluences above $F_{\rm cr}$. Our measurements thus show that broadband measurements of $\epsilon(\omega)$ enable one to distinguish phases that may appear the same based on reflectivity or transmission for a single photon energy at a single angle of incidence.

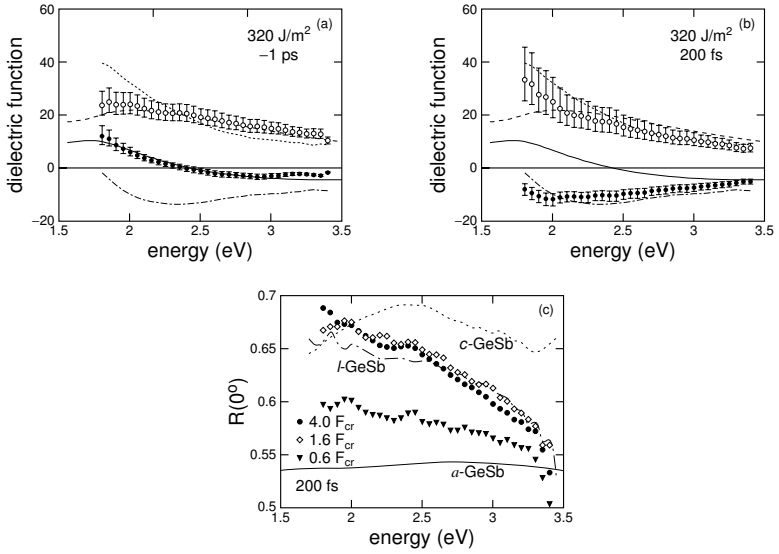

Figure 8. (a),(b) Dielectric function data for a-GeSb thin films — • = Re[$\epsilon(\omega)$], ◦ = Im[$\epsilon(\omega)$]: (a) $\epsilon(\omega)$ under no excitation (-1 ps time delay), and (b) $\epsilon(\omega)$ 200 fs after excitation of 320 J/m^2. In both plots, the solid and dashed curves show the real and imaginary parts of $\epsilon(\omega)$ for the amorphous phase from previous measurements,[J. Solís, 2001] and the dotted and dash-dotted curves show the real and imaginary parts of $\epsilon(\omega)$ of the crystalline phase. (c) Normal-incidence reflectivity calculated from the time-resolved $\epsilon(\omega)$ data. The reflectivity of the amorphous, crystalline, and liquid phases are shown for reference.

4.3 Investigation of a displaced lattice: Coherent phonons in Te

Ultrashort-pulse excitation of Te instantaneously weakens lattice bonding, establishing new equilibrium lattice positions around which the lattice ions vibrate [Cheng et al., 1990, Zeiger et al., 1992, Tangney and Fahy, 2002]. Because the phase of the generated lattice oscillations is the same in the entire pumped volume, probe pulses of shorter duration than the phonon period can be used to observe changes in the optical properties of Te (typically, $\Delta R/R \sim 10\%$) at different degrees of lattice distortion [Cheng et al., 1990, Hunsche et al., 1995]. Experimental work by Bardeen [Bardeen, 1949] and others [Blum and Deaton, 1965] found a pressure-induced semiconductor-to-metal transition in Te. These results coupled with investigations of coherent phonons in other materials [Cheng et al., 1993] suggest that modification or even control of the phase (semiconducting *vs.* semimetallic) of Te is possible at a rate equal to the

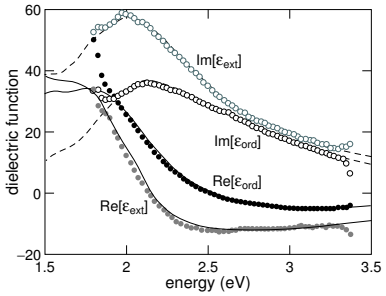

Figure 9. Dielectric tensor data for Te — • = Re[ϵ], ∘ = Im[ϵ]. At −500 fs time delay, both the (a) ordinary and (b) extraordinary dielectric function agree with literature values for the dielectric tensor, represented by the solid and dashed curves. [Palik, 1985]

phonon frequency (≈ 3 THz) for pump fluences below the threshold for permanent damage.

Because Te is uniaxial, two independent elements of the dielectric tensor must be measured to fully characterize the ultrafast material response, as described in Ref. [Roeser et al., 2003]. Figure 9 shows the excellent agreement between measured and literature values [Palik, 1985] of both the ordinary and extraordinary dielectric functions. This agreement not only validates the technique for uniaxial materials, it also shows that no cumulative effects arise from operating in a configuration where the sample is not translated between laser pulses.

The dynamics of $\epsilon_{\mathrm{ord}}(\omega)$ are shown in Figure 10. Within the error of the measurement, dielectric function values remain constant at all times before the pump arrives. After excitation, the oscillatory behavior of the optical properties indicate the presense of coherent phonons. A decaying offset from the initial values, separate from the oscillation, represents the relaxation of the equilibrium lattice spacing as electrons diffuse from the probed region. In contrast to reflectivity-only studies of coherent phonons in materials, the dielectric function data clearly indicate a shift of absorption resonances to lower photon energies. The broad resonance near 2 eV has moved to lower energies, as indicated by the shift in the peak of $\mathrm{Im}[\epsilon_{\mathrm{ord}}(\omega)]$ and the zero of $\mathrm{Re}[\epsilon_{\mathrm{ord}}(\omega)]$. The magnitude and direction of the shift suggest that the lattice may be sufficiently displaced at the peak of the phonon oscillation to cross the conduction and valence bands, but that the short duration of the crossing could prohibit any metallic character from emerging [A. M.-T. Kim et al., 2003]. In addition, we observe larger changes in $\epsilon_{\mathrm{ord}}(\omega)$ than in $\epsilon_{\mathrm{ext}}(\omega)$,

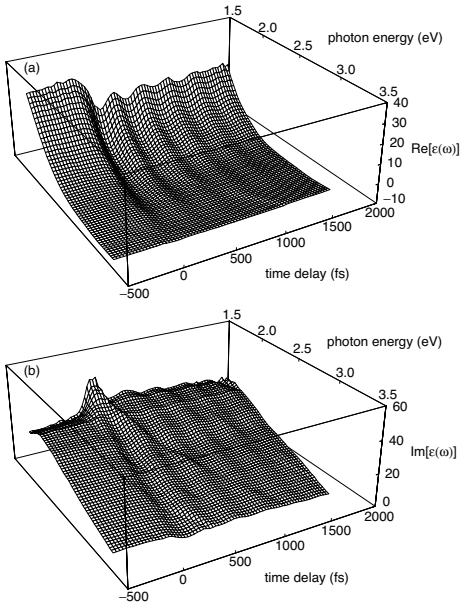

Figure 10. Dynamics of the ordinary dielectric function of Te for excitation with a fluence of 120 J/m^2. Both (a) the real part and (b) the imaginary part show oscillatory behavior due the excitation of coherent phonons.

which may be attributed to the fact that the motion of the coherent phonons is confined to the *ab* plane.

5. Summary

The availability of electronic transitions, the existence of vibrational modes, and the dynamics of nuclei all influence the optical properties of solids. The time-resolved dielectric function measured with this reflectometry technique provides the most information of any linear optical probe, revealing changes in the lattice bonding, carrier distribution, and phase of a material. We avoid the necessity of assuming a particular model of the material dynamics as well as the potential pitfalls of other methods that measure changes in reflectivity at a single photon energy.

Notes

1. Although it seems obvious that transmission and absorption are determined by the "bulk" properties of a solid, this is also true of reflection. While surface quality affects the amount of scattered light, bulk properties determine the amount reflected. This is emphasized in Eq. (8), where a driving term for the generated **D** field is the material polarization created by the applied **E** field.

2. It is apparent from the form of Eq. (10) that electron–electron, electron–phonon, electron–hole, and other multibody interactions are not considered here.

3. The Hamiltonian of Eq. (10), while ignoring important contributions from multibody interactions, captures many of the essential characteristics of semiconductor band structures.

4. Although the coupling term of the Hamiltonian in Eq. (10) is proportional to the field **A**, the material properties experienced by the applied field depend on its direction rather than its magnitude. Any field-strength dependence of the susceptibility results in a fundamentally nonlinear system.

5. The dependence of the dielectric function on the JDOS (Eq. (12)) illustrates how the essential distinction among band structures — their **k**-dependence — is lost in the summation.

6. We take the ions to be fixed in this derivation.

7. For completeness, the parameters of the fit to Te are $\omega_1 = 2.37$ eV, $\Gamma_1 = 1.28$ eV, $f_1 = 105$ eV^2, $\omega_2 = 9.39$ eV, $\Gamma_2 = 4.43$ eV, $f_2 = 170$ eV^2, and an additive constant to the real part of 3.66. The parameters of the fit to GaAs are $\omega_1 = 3.18$ eV, $\Gamma_1 = 0.75$ eV, $f_1 = 38.7$ eV^2, $\omega_2 = 4.67$ eV, $\Gamma_2 = 1.14$ eV, $f_2 = 125$ eV^2, and an additive constant to the real part of 1.85. The real additive constant arises from Kramers–Kronig-type contributions from resonances outside the spectral range of the fit, as discussed in Section 1.3.

8. The real part varies significantly within a linewidth Γ of the resonance frequency ω_0.

9. It is rarely the case that a pump pulse is intense enough to provide one photon for every valence electron in the pumped volume of the solid.

10. This is also representative of the Born-Oppenheimer approximation, where the electronic quantum numbers are the so-called "fast variables" and the nuclear positions are the "slow variables."

11. For an anharmonic excited state potential, the ability to control the end products is reduced, essentially because the projection of a spread nuclear wave function onto the ground state potential can "split" the wave function between the two end products.

12. At densities of 10^{18} cm^{-3}, carrier thermalization occurs within hundreds of femtoseconds [Becker et al., 1988]. Extrapolation of the results of Becker *et al.* [Becker et al., 1988] to 10^{21} cm^{-3} gives a thermalization time on the order of 10 fs.

13. Immediately after photoexcitation, the excited electrons are distributed in the conduction band according to the pump spectrum.

14. In practice, the excitation of 15% of valence electrons to the conduction band is rarely achieved in pump–probe experiments. Excitation of a few percent of valence electrons is both more common and often sufficient to initiate phase transitions.

15. The "fundamental" frequency refers to the center or carrier frequency of the applied **E** field.

16. Here and for the remainder of the discussion we ignore the polarization of the applied **E** field.

17. Many details of phase-matching are omitted here because they are beyond the scope of this article. See Refs. [Boyd, 2003] and [Yariv, 1989].

18. The ease of such a measurement makes it attractive, but it does not fully characterize the temporal profile of the laser pulse [Trebino et al., 1997].

19. For self-focussing, and any other self-action effects, $\omega_1 = \omega_2$.

20. Literature values of $\epsilon(\omega)$ for c-$Ge_{0.06}Sb_{0.94}$ are not available. The data presented are measurements taken in our apparatus of a region of the sample that was permanently crystallized by laser irradiation.

References

[A. M.-T. Kim et al., 2003] A. M.-T. Kim, Roeser, C. A. D., and Mazur, E. (2003). Modulation of the bonding-antibonding splitting in Te by coherent phonons. *Phys. Rev. B*, 68:012301.

[Albrecht et al., 1991] Albrecht, T. F., Seibert, K., and Kurz, H. (1991). Chirp measurement of large-bandwidth femtosecond optical pulses using two-photon absorption. *Opt. Commun.*, 84:223.

[Allen et al., 2000] Allen, R. E., Dumitrica, T., and Torralva, B. (2000). In Tsen, K.-T., editor, *Ultrafast Processes in Semiconductors*. Academic Press, New York.

[Ashcroft and Mermin, 1976] Ashcroft, N. W. and Mermin, N. D. (1976). *Solid State Physics*. Saunders College, Philadelphia.

[Assion et al., 1996] Assion, A., Baumert, T., Helbing, J., Seyfried, V., and Gerber, G. (1996). Coherent control by a single phase shaped femtosecond laser pulse. *Chem. Phys. Lett.*, 259:488.

[Atkins, 1983] Atkins, P. W. (1983). *Molecular Quantum Mechanics*. Oxford University Press, New York.

[Backus et al., 1995] Backus, S., Peatross, J., Huang, C. P., Murnane, M. M., and Kapteyn, H. C. (1995). Ti:sapphire amplifier producing millijoule-level, 21-fs pulses at 1 kHz. *Opt. Lett.*, 20:2000.

[Bardeen, 1949] Bardeen, J. (1949). Pressure change of resistance of tellurium. *Phys. Rev.*, 75:1777.

[Bartels et al., 1998] Bartels, A., Dekorsy, T., Kurz, H., and Köhler, K. (1998). Coherent control of acoustic phonons in semiconductor superlattices. *Appl. Phys. Lett.*, 72:2844.

[Becker et al., 1988] Becker, P. C., Fragnito, H. L., Brito-Cruz, C. H., Fork, R. L., Cunningham, J. E., Henry, J. E., and Shank, C. V. (1988). Femtosecond photon echoes from band-to-band transitions in GaAs. *Phys. Rev. Lett.*, 61:1647.

[Benedict, 2001] Benedict, L. X. (2001). Dielectric function for a model of laser-excited GaAs. *Phys. Rev. B*, 63:075202–1.

[Blum and Deaton, 1965] Blum, F. A. and Deaton, B. C. (1965). Properties of the group VI B elements under pressure. II. Semiconductor-to-metal transition of tellurium. *Phys. Rev.*, 137:A1410.

[Boyd, 2003] Boyd, R. W. (2003). *Nonlinear Optics*. Academic Press, New York, 2nd edition.

[Brixner et al., 2001] Brixner, T., Damrauer, N. H., Niklaus, P., and Gerber, G. (2001). Photoselective adaptive femtosecond quantum control in the liquid phase. *Nature*, 414:57.

[Callan et al., 2001a] Callan, J. P., A. M.-T. Kim, Roeser, C. A. D., and Mazur, E. (2001a). Universal dynamics during and after ultrafast laser-induced semiconductor-to-metal transitions. *Phys. Rev. B*, 64:073201.

[Callan et al., 2001b] Callan, J. P., A. M.-T. Kim, Roeser, C. A. D., Mazur, E., Solis, J., Siegel, J., Afonso, C. N., and de Sande, J. C. G. (2001b). Ultrafast laser-induced phase transitions in amorphous GeSb films. *Phys. Rev. Lett.*, 86:3650.

[Callan et al., 1998] Callan, J. P., Kim, A. M.-T., Huang, L., and Mazur, E. (1998). Ultrafast electron and lattice dynamics in semiconductors at high excited carrier densities. *Chem. Phys.*, 251:167.

[Cavalleri et al., 2001] Cavalleri, A., Tóth, Cs., Siders, C. W., Squier, J. A., Ráski, F., Forget, P., and Kieffer, J. C. (2001). Femtosecond structural dynamics in VO_2 during an ultrafast solid-solid phase transition. *Phys. Rev. Lett.*, 87:237401.

[Cheng et al., 1993] Cheng, T. K., Acioli, L. H., Vidal, J., Zeiger, H. J., Dresselhaus, G., Dresselhaus, M. S., and Ippen, E. P. (1993). Modulation of a semiconductor-to-semimetal transition at 7 THz via coherent lattice vibrations. *Appl. Phys. Lett.*, 62:1901.

[Cheng et al., 1990] Cheng, T. K., Brorson, S. D., Kazeroonian, A. S., Moodera, J. S., Dresselhaus, G., Dresselhaus, M. S., and Ippen, E. P. (1990). Impulsive excitation of coherent phonons observed in reflection in bismuth and antimony. *Appl. Phys. Lett.*, 57:1004.

[Cohen and Chelikowsky, 1989] Cohen, M. L. and Chelikowsky, J. (1989). *Electronic Structure and Optical Properties of Semiconductors*. Springer Verlag, Berlin, 2nd edition.

[de Sande et al., 1994] de Sande, J. C. G., Vega, F., Afonso, C. N., Ortega, C., and Siejka, J. (1994). Optical properties of Sb and SbO_x films. *Thin Solid Films*, 249:195.

[DeCamp et al., 2001] DeCamp, M. F., Reis, D. A., Bucksbaum, P. H., and Merlin, R. (2001). Dynamics and coherent control of high-amplitude optical phonons in bismuth. *Phys. Rev. B*, 74:738.

[Downer et al., 1985] Downer, M. C., Fork, R. L., and Shank, C. V. (1985). Femtosecond imaging of melting and evaporation at a photoexcited silicon surface. *J. Opt. Soc. Am. B*, 2:595.

[Govorkov et al., 1991] Govorkov, S. V., Shumay, I. L., Rudolph, W., and T. Schröder (1991). Time-resolved second-harmonic study of femtosecond laser-induced disordering of GaAs surfaces. *Opt. Lett.*, 16:1013.

[Graves and Allen, 1998] Graves, J. S. and Allen, R. E. (1998). Response of GaAs to fast intense laser pulses. *Phys. Rev. B*, 58:13627.

[Hase et al., 1996] Hase, M., Mizoguchi, K., Harima, H., Nakashima, S., Tani, M., Sakai, K., and Hangyo, M. (1996). Optical control of coherent optical phonons in bismuth films. *Appl. Phys. Lett.*, 69:2474.

[Haus, 1984] Haus, H. A. (1984). *Waves and Fields in Optoelectronics*. Prentice-Hall, Englewood Cliffs, NJ, 1st edition.

[Heller, 1978] Heller, E. J. (1978). Quantum corrections to classical photodissociation models. *J. Chem. Phys.*, 68:2066.

[Heller, 1981] Heller, E. J. (1981). The semiclassical way to molecular spectroscopy. *Acc. Chem. Res.*, 14:368.

[Huang et al., 1998] Huang, L., Callan, J. P., Glezer, E. N., and Mazur, E. (1998). GaAs under ultrafast excitation: Response of the dielectric function. *Phys. Rev. Lett.*, 80:185.

[Hunsche et al., 1995] Hunsche, S., Wienecke, K., Dekorsy, T., and Kurz, H. (1995). Impulsive softening of coherent phonons in tellurium. *Phys. Rev. Lett.*, 75:1815.

[J. Solís, 2001] J. Solís (2001). private communication.

[Jackson, 1975] Jackson, J. D. (1975). *Classical Electrodynamics*. Wiley, New York, 2nd edition.

[Kovalenko et al., 1999] Kovalenko, S. A., Dobryakov, A. L., Ruthmann, J., and Ernsting, N. P. (1999). Femtosecond spectroscopy of condensed phases with chirped supercontinuum probing. *Phys. Rev. A*, 59:2369.

[Misochko et al., 1999] Misochko, O. V., Tani, M., Sakai, K., Nakashima, S., Andreev, V. N., and Chudnovsky, F. A. (1999). Phonons in V_2O_3 above and below the mott transition: a comparison of time- and frequency-domain spectroscopy results. *Physica B*, 263-264:57.

[Palik, 1985] Palik, E. D. (1985). *Handbook of Optical Constants of Solids*. Academic Press, New York.

[Rice and Zhao, 2000] Rice, S. A. and Zhao, M. (2000). *Optical Control of Molecular Dynamics*. John Wiley and Sons, New York.

[Roeser et al., 2003] Roeser, C. A. D., Kim, A. M.-T., Callan, J. P., Huang, L., Glezer, E. N., Siegal, Y., and Mazur, E. (2003). Femtosecond time-resolved dielectric function measurements by dual-angle reflectometry. *Rev. Sci. Instrum.*, 74:3413.

[Saeta et al., 1991] Saeta, P., Wang, J.-K., Siegal, Y., Bloembergen, N., and Mazur, E. (1991). Ultrafast electronic disordering during femtosecond laser melting of GaAs. *Phys. Rev. Lett.*, 67:1023.

[Shah, 1996] Shah, J. (1996). *Ultrafast Spectroscopy of Semiconductors and Semiconductor Nanostructures*. Springer-Verlag, Berlin.

[Shank et al., 1983a] Shank, C. V., Yen, R., and Hirlimann, C. (1983a). Femtosecond-time-resolved surface structural dynamics of optically excited silicon. *Phys. Rev. Lett.*, 51:900.

[Shank et al., 1983b] Shank, C. V., Yen, R., and Hirlimann, C. (1983b). Time-resolved reflectivity measurements of femtosecond-optical-pulse-induced phase transitions in silicon. *Phys. Rev. Lett.*, 50:454.

[Sokolowski-Tinten et al., 1998] Sokolowski-Tinten, K., Bialkowski, J., Cavalleri, A., von der Linde, D., Oparin, A., Meyer-ter-Vehn, J., and Anisimov, S. I. (1998). Transient states of matter during short pulse laser ablation. *Phys. Rev. Lett.*, 81:224.

[Sokolowski-Tinten et al., 1998] Sokolowski-Tinten, K., Blome, C., Blums, J., Cavalleri, A., Dietrich, C., Tarasevitch, A., Uschmann, I., Förster, E., Kammler, M., Horn-von-Hoegon, M., and von der Linde, D. (1998). Femtosecond x-ray measurement of coherent lattice vibrations near the Lindemann stability limit. *Nature*, 81:3679.

[Sokolowski-Tinten et al., 1998] Sokolowski-Tinten, K., J. Solís, Bialkowski, J., Siegel, J., Afonso, C. N., and von der Linde, D. (1998). Dynamics of ultrafast phase changes in amorphous GeSb films. *Phys. Rev. Lett.*, 81:3679.

[Sokolowski-Tinten et al., 1991] Sokolowski-Tinten, K., Schulz, H., Bialkowski, J., and von der Linde, D. (1991). Two distinct transitions in ultrafast solid-liquid phase transformations of GaAs. *Appl. Phys. A*, 53:227.

[Stampfli and Bennemann, 1990] Stampfli, P. and Bennemann, K. H. (1990). Theory for the instability of the diamond structure of Si, Ge, and C induced by a dense electron-hole plasma. *Phys. Rev. B*, 42:7163.

[Stampfli and Bennemann, 1994] Stampfli, P. and Bennemann, K. H. (1994). Time dependence of the laser-induced femtosecond lattice instability of Si and GaAs: Role of longitudinal optical distortions. *Phys. Rev. B*, 49:7299.

[Tangney and Fahy, 2002] Tangney, P. and Fahy, S. (2002). Density-functional theory approach to ultrafast laser excitation of semiconductors: Application to the a_1 phonon in tellurium. *Phys. Rev. B*, 65:054302.

[Tannor et al., 2086] Tannor, D. J., Kosloff, R., and Rice, S. A. (2086). Coherent pulse sequence induced control of selectivity of reactions: Exact quantum mechanical calculations. *J. Chem. Phys.*, 85:5805.

[Tom et al., 1988] Tom, H. W. K., Aumiller, G. D., and Brito-Cruz, C. H. (1988). Time-resolved study of laser-induced disorder of Si surfaces. *Phys. Rev. Lett.*, 60:1438.

[Trebino et al., 1997] Trebino, R., DeLong, K. W., Fittinghoff, D. N., Sweetser, J. N., M. A. Krumbügel, Richman, B. A., and Kane, D. J. (1997). Measuring ultrashort laser pulses in the time-frequency domain using frequency-resolved optical gating. *Rev. Sci. Instrum.*, 68:3277.

[Wefers et al., 1995] Wefers, M. W., Kawashima, H., and Nelson, K. A. (1995). Optical control over femtosecond polarization dynamics. *J. Phys. Chem. Solids*, 57:1425.

[Yariv, 1989] Yariv, A. (1989). *Quantum Electronics*. Wiley, New York, 3rd edition.

[Yu and Cardona, 1996] Yu, P. Y. and Cardona, M. (1996). *Fundamentals of Semiconductors*. Springer-Verlag, Berlin.

[Zeiger et al., 1992] Zeiger, H. J., Vidal, J., Cheng, T. K., Ippen, E. P., Dresselhaus, G., and Dresselhaus, M. S. (1992). Theory for displacive excitation of coherent phonons. *Phys. Rev. B*, 45:768.